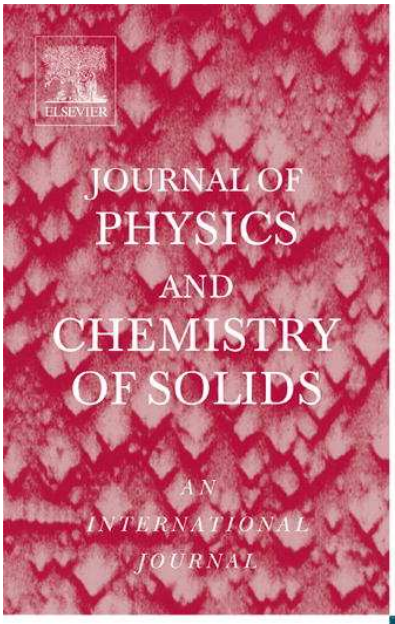

VOLUME 69 No. 1 ISSN 0022-3697
2008 JANUARY

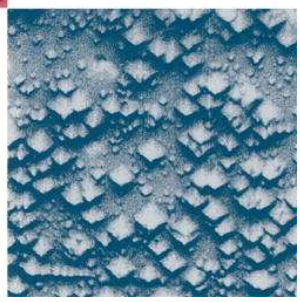

Available online at www.sciencedirect.com
ScienceDirect
Journal of Physics and Chemistry of Solids 69 (2008) 168–181
JOURNAL OF PHYSICS AND CHEMISTRY OF SOLIDS
www.elsevier.com/locate/jpcs

Vibrational and thermodynamic properties of metals from a model embedded-atom potential

Qiuping Bian, S.K. Bose*, R.C. Shukla

Physics Department, Brock University, St. Catharines, Ont., Canada L2S 3A1

Received 22 May 2007; received in revised form 3 July 2007; accepted 16 August 2007

Abstract

This work provides the first systematic test of validity of the embedded-atom potentials of Mei et al. [Phys. Rev. B 43 (1991) 4653], via a complete study of the vibrational and thermodynamic properties of isoelectronic transition (Ni, Pd, Pt) and noble (Cu, Ag, Au) metals. Phonon dispersion curves and thermal properties are studied within the quasiharmonic approximation. Results for the temperature-dependence of the lattice constants, coefficients of linear thermal expansion, isothermal and adiabatic bulk moduli, heat capacities at constant volume and constant pressure, Debye temperatures and Grüneisen parameters are presented. Electronic contribution to the specific heat is included explicitly via density-functional calculation. The calculated phonon frequencies for Ag and Cu agree well with the results from inelastic neutron scattering experiments. Despite less satisfactory agreement between calculated and measured phonon frequencies for the other four metals, isothermal and adiabatic bulk moduli and the specific heats of all metals are reproduced reasonably well by the model, while the Grüneisen parameter and Debye temperature are underestimated by about 10%. The coefficient of linear thermal expansion is underestimated with respect to measured values in most cases except for Pt and Au. The results are good for Pt up to 1000 K and for Au up to 500 K.

Keywords: A. Metals; C. Semi-empirical/ab initio method; D. Lattice dynamics and thermodynamic properties

1. Introduction

The inadequacy of volume-independent pair-potentials to describe metallic cohesion is well-known and has been adequately documented [1,2]. Various approaches, at varying levels of sophistication, have been used to address the volume-dependence of the energy of a metallic system originating from the presence of the interacting electron gas. These range from using volume-dependent parameters in the pair potential itself [3] to writing the total energy as a sum of pair potentials plus an empirical volume/density-dependent term [4–6] or an electronic band(bond) energy term [7]. The latter is often written in terms of the first few moments of the electronic density of states (DOSs) in the tight-binding approximation [8]. For transition metals, invoking a simplified model of rectangular *d*-DOSs due to Friedel, the bond energy term is sometimes approximated simply via the second moment of the DOSs [9–11].

An approach which provides, in principle, a considerable improvement over the pair-potential model is the embedded-atom method (EAM) [4,12], where the volume-dependence of the energy is explicitly incorporated via electron density. In EAM the energy of the metal is viewed as the energy to embed an atom into the local electron density provided by the remaining atoms of the system, plus a sum of pair interaction potentials between the atoms. This method, which was developed by Daw and Baskes [12], and almost simultaneously by Finnis and Sinclair [4], starts with the ansatz:

$$E_{tot} = \sum_i F_i(\rho_{h,i}) + \frac{1}{2}\sum_{\substack{i,j \\ (i\neq j)}} \Phi(R_{ij}), \tag{1}$$

$$\rho_{h,i} = \sum_{j(j\neq i)} f_j(R_{ij}), \tag{2}$$

*Corresponding author. Tel.: +1 905 688 5550/3876; fax: +1 905 984 4857.
E-mail address: sbose@brocku.ca (S.K. Bose).

0022-3697/$ - see front matter © 2007 Elsevier Ltd. All rights reserved.
doi:10.1016/j.jpcs.2007.08.046

where E_{tot} is the total internal energy, $\rho_{h,i}$ is the host electron density at the atom at site i due to all other atoms, f_j is the electron density of the atom at site j as a function of distance from its center, R_{ij} is the separation distance between atoms at sites i and j. The function $F_i(\rho_{h,i})$, called the embedding energy, is the energy to embed the atom at site i in an electron density $\rho_{h,i}$. Φ_{ij} is a two-body central pair potential between atoms at sites i and j. The host electron density $\rho_{h,i}$ is assumed to be a linear superposition of spherically symmetric contributions from all individual atoms except the atom at site i. For a crystalline solid with one atom per unit cell, there is no host-guest distinction, and the embedding function and the electron density do not have any site-dependence, i.e. $F_i = F$, $\rho_{h,i} = \rho$, $f_j = f$.

In the model proposed by Finnis and Sinclair [4] the total energy of a system of atoms is assumed to consist of a binding term proportional to the square-root of the local density and a repulsive pairwise potential term. Another approach to this type of theory was provided by Manninen [13], Jacobsen et al. [14], who derived the functional form of the two terms in Eq. (1) by using the density functional theory. Although Daw and Baskes [12] had also used the density functional theory to justify the use of Eq. (1), in most applications of the method the two terms of Eq. (1) were written in terms of parameters that were fitted to observed properties of the system. In this sense, the EAM remains an empirical or at best a semi-empirical method. However, the simplicity and ease with which it could be applied to a large variety of situations has led to its wide use in the study of liquids, alloys, surfaces and interfaces, impurities and other defects in solids.

Foiles [15] has applied the EAM to compute the static structure factor and theoretical pressure at the experimental zero pressure density for several liquid transition metals. Mei and Davenport [16] used the EAM and molecular dynamics simulation to study the co-efficients of self-diffusion for several liquid metals. These authors [17] have also computed the Gibbs free energy of solid and liquid Al using the EAM and studied melting/freezing in Al via crystal-liquid interface simulation. Foiles et al. [18] have studied the vacancy formation and migration energies in several elemental metals and their alloys. Johnson [19] has used the EAM to calculate heats of formation of a large number of binary alloys. There are a large number of surface and interface studies [20–29] involving the EAM by Daw, Nelson, Foiles, Baskes and co-workers. Readers interested in the formulation and applications of the EAM method should consult the review article by Daw et al. [30]. Relevant to the present work is the work of Foiles and Adams [31], who studied the six fcc metals: Cu, Ag, Au, Ni, Pd and Pt for their solid and liquid phase Gibbs free energies, melting points and thermal expansion using the EAM potentials developed by Foiles et al. [18].

By replacing the atomic electron density with an exponentially decaying function, Johnson [19] developed a set of analytic EAM functions for the nearest-neighbor model of six fcc metals: Ni, Pd, Pt, Cu, Ag, and Au. However, this model had the limitation that all materials were forced to have the same anisotropy ratio of the shear moduli: $c_{44}/(c_{11} - c_{12}) = 1$. Oh and Johnson [32] extended the model beyond nearest neighbors, at the cost of sacrificing the simple analytic form. Mei et al. [33] have overcome this challenge and extended this nearest-neighbor model into one in which the embedded-atom potentials are analytic and valid for any choice of the cut-off distance. In particular they derived the values of the parameters for their EAM potential and density functions for the same six fcc metals and used the model in a molecular dynamics study of thermal expansion and specific heat of liquid Cu as a function of temperature. In later studies they applied the model to study self-diffusion in the liquid phase of the above six metals [16] and the melting in Al [17]. Kuiying et al. [34] have used this EAM potential in a molecular dynamics study of the local structure in supercooled liquid and solid Cu and Al.

An attractive feature of the model used by Mei et al. [33] is that the repulsive potential is chosen in the same Rydberg form as the total energy. The Rydberg form of the total energy is known to yield the so-called *universal* equation of state for metals, as was confirmed by Rose et al. [35] in a study involving a large number of metallic systems. Earlier Varshni and Bloore [36] had found that two-body potentials of the Rydberg form were more suitable than Morse-type potentials in reproducing the equation of state of solid Cu, Ag and Ni.

Although the parameters of EAM potential have been almost always determined by fitting to bulk crystal data [18,19,33], their applications have usually been confined to the studies of impurities, vacancies, surfaces and interfaces. In most cases thorough studies of bulk crystalline properties, such as the vibrational [20–22] and thermodynamic properties, have not been carried out. Such studies can provide important information about the general effectiveness of the models to the community of researchers involved in the application of the EAM to the study of metallic systems.

The goal of this work is not to present new/improved results for the vibrational and thermodynamic properties of the bulk crystalline phase of elemental metals, but to provide an idea as to how well/poorly the EAM model of Mei et al. [33] (and other EAM models with similar parametrization schemes) does in this respect. This is an issue which has not been adequately addressed so far. Via extensive calculations of the phonon dispersion and a complete study of the thermodynamic properties, this work points out, for the first time, the advantages as well as the limitations of the EAM method for the study of metals in general. Conclusions reached in this work (Section 5) are expected to be valid for all EAM models similar to the model of Mei et al. [33] in terms of the number and physical nature of the adjustable parameters used.

2. The model

In the model of Mei et al. [33], as in any EAM, there are two components to the total energy: a two-body potential

$\Phi(R)$ and the embedding function $F(\rho)$. Here R is the nearest neighbor separation and ρ is the atomic electron density at the distance R. $F(\rho)$ constitutes the volume-dependent part of the energy, essential for a metallic system. The choice of the two-body potential is somewhat arbitrary and Mei et al. [33] chose the Rydberg form, guided by the result of Rose et al. [35], who had shown that the relationship between the total energy and the nearest neighbor distance of a large number of metals could be fitted to this form: the so-called "universal equation of state". The Rydberg form of the total energy as well as the two-body potential $\Phi(R)$ as a function of the nearest neighbor distance in Eq. (1) leads to the following form of the embedding function $F(\rho)$ [33]:

$$F(\rho) = -E_c\left[1-\frac{\alpha}{\beta}\ln\left[\frac{\rho}{\rho_e}\right]\right]\left[\frac{\rho}{\rho_e}\right]^{\alpha/\beta} + \frac{1}{2}\phi_e\sum_{\Lambda} s_\Lambda \exp[-(p_\Lambda-1)\gamma] \times\left[1+(p_\Lambda-1)\delta - p_\Lambda\frac{\delta}{\beta}\ln\left[\frac{\rho}{\rho_e}\right]\right]\left[\frac{\rho}{\rho_e}\right]^{p_\Lambda\gamma/\beta}, \quad (3)$$

where the constants δ, γ and ϕ_e define the two-body potential:

$$\Phi(R) = -\phi_e[1+\delta(R/R_{1e}-1)]\exp[-\gamma(R/R_{1e}-1)], \quad (4)$$

and E_c is the cohesive energy of the solid. The Rydberg form of the total energy dictates that the constant α be related to the cohesive energy E_c, the equilibrium (minimum energy) values of the Bulk modulus B_e and atomic volume Ω_e as $\alpha = (9B_e\Omega_e/E_c)^{1/2}$. In the work of Mei et al. [33], the charge density ρ at a distance R was represented as a sum of inverse power polynomial in the distance R

$$\rho = \sum_{\Lambda} s_\Lambda f(R_\Lambda), \quad f(R) = f_e\sum_{\tau=0}^{\kappa} c_\tau (R_{1e}/R)^\tau. \quad (5)$$

s_Λ in Eq. (5) is the number of atoms on the Λth neighbor shell with respect to a given reference atom. p_Λ refers to the Λth neighbor shell via $R_\Lambda = p_\Lambda R_1, \Lambda = 1,2,\ldots$, where R_Λ is the distance of the Λth-neighbor shell. The constants p_Λ depend on the crystal structure type: for the fcc structure $p_\Lambda = \sqrt{\Lambda}$. In Eqs. (3)–(5), the subscript e refers to the equilibrium value, i.e. R_{1e} is the equilibrium nearest neighbor distance, ρ_e is the charge density at the distance R_{1e}, and f_e is just a constant. Only ratios of electronic densities appear in Eq. (3) and hence ρ_e cancels out. The constant f_e was set equal to $\rho_e/12$.

Mei et al. [33] used $\kappa = 5$ in Eq. (5) and determined the constants $c_0 - c_5$ by fitting to the atomic charge density ρ. The remaining parameters β, γ and δ were obtained by fitting to the measured values of unrelaxed vacancy formation energy and the elastic constants, all of which were calculated by using three shells of neighbors for all the fcc metals considered. The exact details of the fitting procedure used are given in Ref. [33].

The values of the constants thus generated and given in Table 1 of Mei et al. [33], were used in the present work with one notable difference. Mei et al. [33] obtained the values of the parameters in their model by considering three shells of neighbors for the fcc solid. In the molecular dynamics study of liquid and solid Cu, they used a cut-off distance in their embedding function and pair-potential lying between the third and the fourth nearest neighbors. We have calculated the elastic constants C_{11}, C_{12} and C_{44} using the homogeneous deformation method and also from the long wavelength phonons and we have studied their variation with respect to the number of neighbor shells included in the calculation. For three shells of neighbors our results obtained via the homogeneous deformation method agrees well with those obtained by Mei et al. [33]. However, the values obtained via the homogeneous deformation method and from long wavelength phonons differ significantly from each other as well as from the experimental values. The differences in the results obtained by the two methods, as well as between the calculated and experimental values, decrease on increasing the number of neighbor shells in the calculation and practically disappear as the number of neighbor shells reaches six. Based on this result, we have calculated the phonon spectra and all the physical properties by using six shells of neighbors for this model of EAM. We have compared the phonon frequencies for the test case of Cu by using three to six shells of neighbors. The maximum difference, which is found for low energy phonons, between the three and six neighbor shells is of the order of 1%. The differences in the phonon frequencies between the three and six neighbor shell calculations decrease with increasing wave vector, and at the zone boundary they are of the order of .01%. The static energy of the solid, given by Eq. (1), changes by ~0.7% as the number of shells increases from three to six. However, there is virtually no change in the location of the minimum in the static energy as a function of lattice parameter, as well as the curvature at the location of the minimum.

3. Phonons

The phonon spectra were calculated by diagonalizing the dynamical matrix, obtained from the Fourier transform of the force constant tensor $\mathbf{\Phi}_{ij}(l,m)$ given by

$$\mathbf{\Phi}_{ij}(l,m) = \frac{\partial^2 E_{tot}}{\partial R^i(l)\,\partial R^j(m)}, \quad (6)$$

where l,m are the labels of the atoms. For E_{tot} given by Eqs. (1) and (2), and with $l \neq m$

$$\mathbf{\Phi}_{ij}(l,m) = -F_l'(\rho_l)f_m''(R_{lm})\frac{R_{lm}^i R_{lm}^i}{R_{lm}^2} - F_m'(\rho_m)f_l''(R_{lm})\frac{R_{lm}^j R_{lm}^i}{R_{lm}^2}$$

$$
\begin{aligned}
&- \Phi''(R_{lm})\frac{R^i_{lm}R^i_{lm}}{R^2_{lm}} - [F'_l(\rho_l)f'_m(R_{lm}) \\
&+ F'_m(\rho_m)f'_l(R_{lm}) + \Phi'(R_{lm})] \\
&\times\left\{\frac{\delta_{ij}}{R_{lm}} - \frac{R^i_{lm}R^j_{lm}}{R^3_{lm}}\right\} + \sum_{n(\neq l,m)} F''_n(\rho_n) \\
&\times f'_l(R_{ln})f'_m(R_{mn})\frac{R^j_{mn}}{R_{mn}}\frac{R^i_{ln}}{R_{ln}}, \qquad (7)
\end{aligned}
$$

where the prime in the function in the above equation denotes the derivative of the function with respect to its argument. Though written somewhat differently, the above expression is in agreement with that derived by Finnis and Sinclair [4].

The calculated phonon frequencies for the six fcc metals Ni, Pd, Pt and Cu, Ag, Au are plotted in Figs. 1–6. In Fig. 1 we compare the calculated phonon spectrum of Cu with the experimental results of Svensson, Brockhouse and Rowe [37]. The squares and the circles represent the phonon frequencies from the inelastic neutron scattering (INS) experiment at room temperature (296 K), while the solid line denotes the calculated spectrum. For estimating the importance of the embedding term we have used dashed lines to show the frequencies obtained by considering only the pair potential term, i.e., neglecting the contribution from the embedding function. The pair potential and the embedding terms contribute to the force constant with opposite signs: without the embedding term the phonon frequencies at high values of the wave vectors would have much worse agreement with the measured frequencies.

We find that the three-body terms coming from the embedding function (the last term in Eq. (7)) have a very small effect on the phonon frequencies for large wave vectors, the values obtained with and without these terms

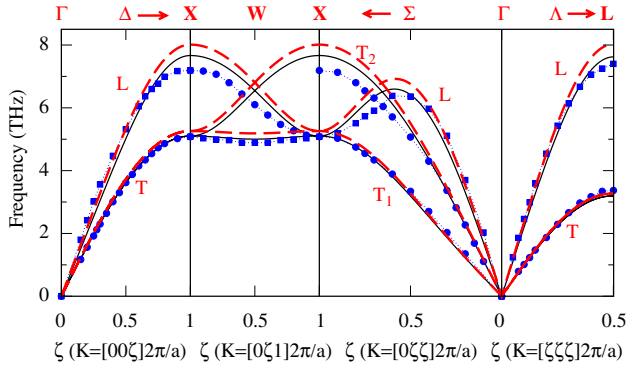

Fig. 1. Phonon dispersion curves for Cu. The solid lines represent the calculated phonon dispersion curves at the room temperature equilibrium lattice parameter of 3.6131 Å [53]. The dashed lines denote the phonon dispersion curves obtained by using only the pair potential term, i.e. without the contribution from the embedding function. The square and round points are the experimental data at 296 K from Ref. [37]. The symbol L represents the longitudinal branch, and the symbols T, T_1 and T_2 represent transverse branches.

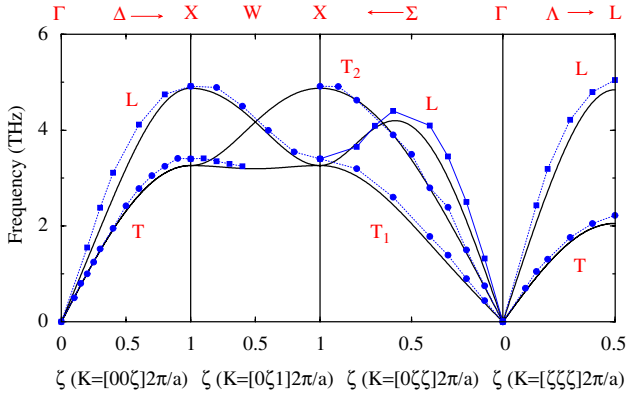

Fig. 2. Phonon dispersion curves for Ag. The solid lines are the calculated phonon dispersion curves at the room temperature equilibrium lattice parameter [53]. The square and round points are the experimental data from Ref. [46] at room temperature. L, T, T_1 and T_2 carry the same meanings as in Fig. 1.

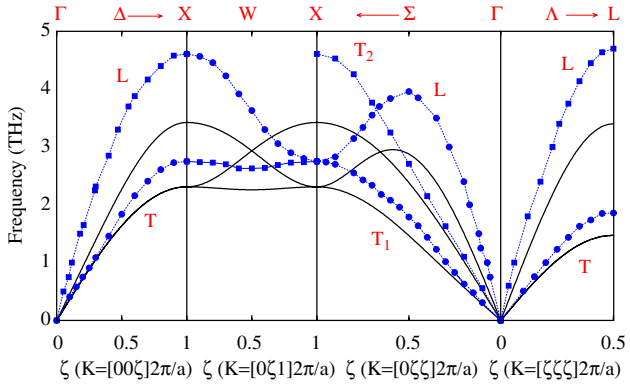

Fig. 3. Phonon dispersion curves for Au. The solid lines, square and round points and the symbols L, T, T_1 and T_2 carry the same meanings as in Figs. 1 and 2. The experimental data at 296 K is from Ref. [54]

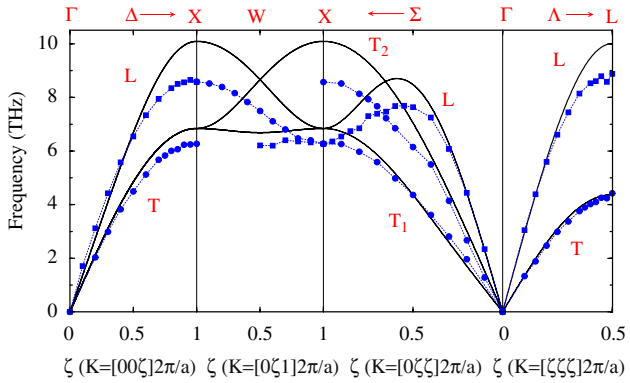

Fig. 4. Phonon dispersion curves for Ni. The solid lines, square and round points and the symbols L, T, T_1 and T_2 carry the same meanings as in Figs. 1 and 2. The experimental data taken at 296 K is from Ref. [55].

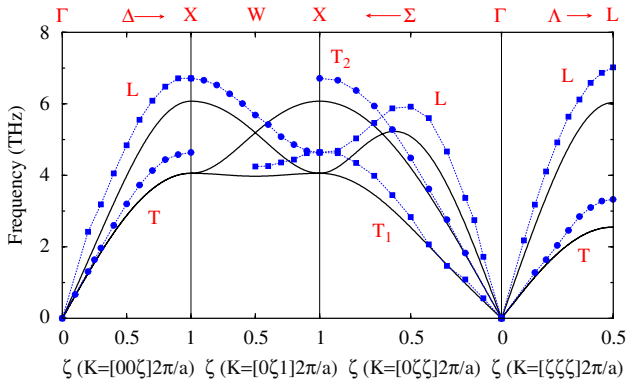

Fig. 5. Phonon dispersion curves for Pd. The solid lines, square and round points and the symbols L, T, T_1 and T_2 carry the same meanings as in Figs. 1 and 2. The experimental data taken at 120 K is from Ref. [56].

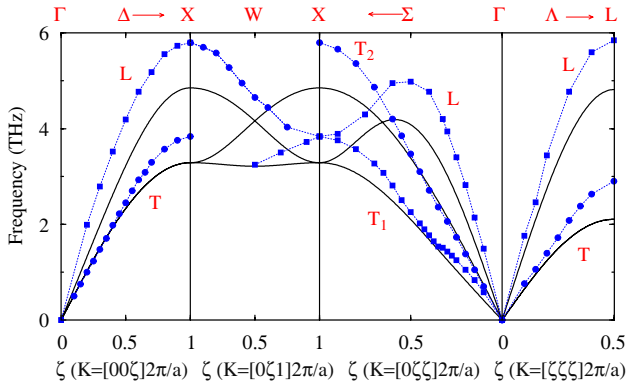

Fig. 6. Phonon dispersion curves for Pt. The solid lines, square and round points and the symbols L, T, T_1 and T_2 carry the same meanings as in Figs. 1 and 2. The experimental data is from Ref. [43].

are almost indistinguishable. Near the zone center, where the phonon frequencies themselves are very small, the relative contribution of the three-body term is somewhat larger. This is consistent with the fact that the three-body terms break the Cauchy relation: $C_{44} = C_{12}$. It is well-known that if the total energy is written strictly as a sum of two-body potentials, then the elastic constants obey the Cauchy relation: $C_{44} = C_{12}$ [38]. The deviation from the Cauchy relation, which most solids exhibit to some extent, can only be obtained by including three- and other many-body interactions in the energy. It is the last term in Eq. (7) that provides the three-body term necessary to break the Cauchy relation. Its effect on phonon frequencies is manifest only near the zone boundary, changing the slopes of the phonon dispersion curves and thus affecting the elastic constants.

We have also compared the calculated phonon frequencies of Cu with the experimental values for off-symmetry wave vectors, as given by Nilsson and Ronaldson [39]. The agreement is similar to that for the wave vectors along the symmetry directions, in the sense that the agreement is very good for small wave vectors, while becoming progressively worse with increasing wave vectors to the same extent as for the symmetry direction wave vectors shown in Fig. 1.

The terms involving the total embedding function in Eq. (1) contribute about $\frac{1}{4}$ to $\frac{1}{3}$ of the total energy for the model of Mei et al. [33], but their contribution to vibrational frequencies is less than 10%. Hence, the embedding term contributes to the temperature variation of thermodynamic properties mainly via the static part of the free energy.

For Cu the phonon frequencies calculated by considering only the contributions from the nearest neighbors in the fcc structure produce about 90% of the final converged frequencies originating from all neighbors. This is in agreement with the observation of Svensson et al. [37], who used several Born–von Kármán force constant models involving neighbors up to various different shells to study the agreement between the calculated phonon frequencies and those from the INS experiment. Their least square fits of atomic and planar force constants to the observed phonon frequencies indicate that the nearest-neighbor forces dominate in Cu, although longer-range forces extending at least to the sixth-nearest neighbors are needed for a complete agreement between the calculated and experimental frequencies. A similar result was found by Nilsson and Ronaldson [39] in their INS study of phonon frequencies in Cu at wave vectors of both symmetry and off-symmetry points in the Brillouin zone at a temperature of 80 K.

Among the six fcc metals, the agreement between the calculated and experimental phonon spectra is almost perfect for Ag and only slightly less so for Cu. For all other metals the agreement becomes increasingly worse with increasing wave vectors in all the symmetry directions, the worst case being that of Au. For Pd, Pt and Au the calculated phonon frequencies are underestimated with respect to the experimental results, while they are somewhat overestimated for Ni. For Cu [21], Ag [22], Ni and Pd [20], this trend as well as the level of agreement between the calculated and experimental phonon frequencies is the same as in the EAM scheme of Daw and Baskes [12], where the total charge density at an atomic location is calculated from the *ab initio* Hartree–Fock results for free atom charge densities. Of course, if one is simply interested in the phonon spectra, Born–von Kármán fit to force constants can yield very satisfactory results [37]. Note that the agreement with the experimental phonon spectra for Cu obtained by Cowley and Shukla [3] by using a nearest-neighbor Born–Mayer potential with volume-dependent prefactor is as good as that obtained in the present EAM model. The total energy of the crystal in this study by Cowley and Shukla [3] consisted of kinetic, exchange and correlation energies of the electron gas and an electron–ion interaction term in addition to the nearest-neighbor Born–Mayer potential.

As pointed out by Daw and Hatcher [20], as long as the fitting is done primarily to elastic constants, which involve phonons near the zone center only, the agreement for high

frequency phonons near the zone boundary is not guaranteed. In this respect, phonons calculated via *ab initio* electronic structure methods, which can capture the details of Fermi surface topology without resorting to any empirical fitting procedure, can yield superior results [40,41], although results do vary depending on the method of electronic structure calculation and details of the implementation of exchange-correlation potentials, etc. [42]. For the test case of Cu studied by Mishin et al. [41], *ab initio* tight-binding results for high frequency phonons are superior to those generated by the two EAM schemes studied by these authors. The importance of the Fermi surface topology is particularly evident in the phonon spectrum of Pd and Pt, where pronounced Kohn anomalies, discussed in detail by Dutton et al. [43], can be seen in the T_1 branch in the symmetry direction $\Gamma \rightarrow X$ via Σ (see Figs. 5 and 6). Kohn anomalies are kinks in the phonon dispersion curves resulting from the interaction of conduction electrons with lattice vibrations and are directly related to sharp peaks in the number of (final and initial) electronic states connected by a given phonon wave vector $\mathbf{q}$. Calculations based on the EAM methods, where no Fermi surface-related information enters the theory, fail to capture Kohn anomalies and possibly some other important features of the phonon spectrum. Note that results for Pd obtained by Savrasov and Savrasov [40] using *ab initio* electronic structure method (full potential linear muffin-tin orbitals and linear response) show almost perfect agreement with the experimental results.

Mishin et al. [44] have used the EAM to compute the phonon spectra in Ni, with results that show almost perfect agreement with the INS data. Their superior results, much better than those obtained in the present work or by Daw and Hatcher [20] using the EAM potential of Daw and Baskes [12], are due to the fact that in determining the parameters in the EAM potential they fit, among many other properties, the zone boundary phonons at the X point. Chantasiriwan and Milstein [45] have used the EAM to compute the phonon spectrum in Cu, Ag, Au and Ni and several other metals and obtain a very good agreement with the INS data, only at the cost of using 21 parameters in their model, which are fitted to various crystal properties. In contrast, the model of Mei et al. has effectively four parameters, as the constants $c_0 - c_5$ are used to represent the charge density in the polynomial form involving inverse powers of r. It is worth noting that though there is quantitative disagreement between the calculated and the INS results for Ni, Au, Pd and Pt, there is no disagreement in the shape of the phonon dispersion curves, which is reproduced well for all six metals. Experimentalists have tried to explain the differences among various metals by appealing to the so-called criterion of homology of forces [46] between metals A and B: $v_A/v_B = \sqrt{(Ma^2)_B}/\sqrt{(Ma^2)_A}$, where v, M, and a refer to the phonon frequency, atomic mass, and lattice parameter, respectively. It would be meaningful to apply the criterion within a given group, e.g. transition or noble metals. Kamitakahara and Brockhouse [46] find that the rule works well for various zone boundary symmetry points for Cu and Ag. The calculated frequencies for Cu and Ag obey the rule, but to a slightly lesser degree. For Cu and Au, measured phonon frequencies in the symmetry direction $\Gamma \rightarrow X$ show small deviation from the homology rule for the transverse branch, but significant deviation for the longitudinal branch. The deviation from the homology rule in the measured frequencies for the transition metals Ni, Pd and Pt, is more pronounced than for the noble metals. Calculated frequencies also show significant deviation from the homology rule, with a trend which is opposite to that for the measured frequencies. If a ratio of the measured frequency values is less than that given by the homology rule, then for the calculated values it is higher. The extent of the deviation for calculated frequencies is no worse than that revealed by the measured frequencies. For the calculated frequencies one exception is the pair Ni and Pt, for which they seem to obey the homology rule to within 2%. The measured frequency ratios for Ni and Pt deviate from the homology rule by 20–30%. These results indicate that the important role played by the *d*-electrons for the bonding in transition metals is not captured by the EAM. For noble metals the effect of the filled or almost filled *d*-shell on bonding is less pronounced. Stronger deviation in case of gold may be due to relativistic effects (which is known to result in increased *s–d* hybridization), not accounted for in the EAM.

4. Thermodynamic properties

In the quasiharmonic approximation, the total Helmholtz free energy of the crystal at temperature T and volume V or lattice constant a is given by

$$F(a,T) = E_{tot}(a) + k_B \sum_{\mathbf{K}s} \ln\left\{2\sinh\frac{\hbar\omega_s(\mathbf{K},a)}{2k_BT}\right\}, \tag{8}$$

where E_{tot} is the static total energy given by Eq. (1) at a given volume V or lattice constant a. $\omega_s(\mathbf{K},a)$ is the frequency of sth mode for a given wave vector $\mathbf{K}$ and lattice constant a. All thermodynamic properties are calculated from the free energy given by Eq. (8). In obtaining the wave vector sum in Eq. (8) we consider a 20^3 uniform grid in the Brillouin zone (BZ) giving 256 wave vectors in the irreducible part. The sum is performed using these 256 wave vectors, appropriately weighted according to the point-group symmetry of the fcc solid. Temperature variation of thermodynamic properties is studied from 0 to 1400 K in steps of 2 K.

At a given temperature T, the equilibrium lattice parameter is determined by the minimum of $F(a,T)$ with respect to a. The variation of lattice constant with temperature for the six fcc metals is shown in Fig. 7. It should be noted that our quasiharmonic results for Cu agree very well with those obtained by Mei et al. [33] using molecular dynamics simulation, which includes

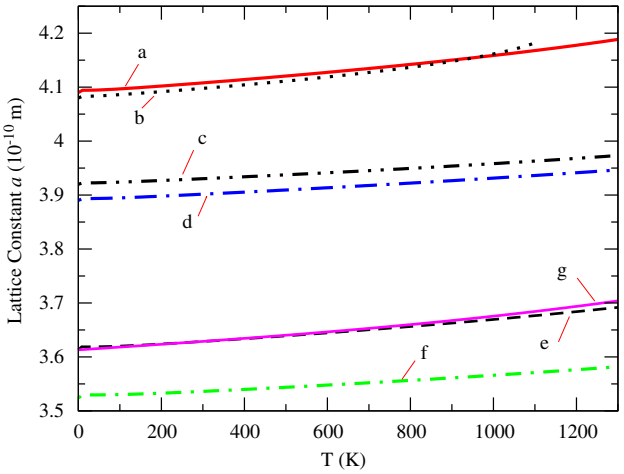

Fig. 7. Lattice constant against temperature for the six fcc metals. Line a is for Ag, b is for Au, c is for Pt, d is for Pd, e is for Cu, and f is for Ni. Line g denotes the results of the MD simulation Mei et al. [33] for Cu.

anharmonic effects to all order. A small difference, increasing with temperature, appears above 900 K due to the absence of explicit anharmonic effects in our quasi-harmonic calculations. The results for all six metals are as good as those obtained by Foiles and Admas [31] using the EAM potentials of Foiles et al. [18].

The coefficient of linear thermal expansion is given by

$$\alpha(T) = \frac{1}{a_e(T)}\left(\frac{\mathrm{d}a_e(T)}{\mathrm{d}T}\right)_p. \tag{9}$$

In experimental works $a_e(T)$ in Eq. (9) is often replaced with [47,48] $a_e(T_c)$, where T_c is a reference temperature, usually taken to be the room temperature. To be consistent with experimental and other theoretical work [47], we consider Eq. (9) with $a_e(T) = a_e(T_c)$; $T_c = 293$. The coefficients of linear expansion $\alpha(T)$ calculated for the six fcc metals are shown in Figs. 8–10 along with the experimental values. Thermal expansion coefficients for Cu, Ag and Ni calculated by Shukla and MacDonald [48] and MacDonald and MacDonald [47] based on empirical nearest-neighbor central force model and incorporating two lowest-order, cubic and quartic, anharmonic effects show much better agreement with experiment than those given by the present EAM model in the quasiharmonic approximation.

The isothermal bulk modulus at a temperature T is given by

$$B(T) = V\left(\frac{\partial^2 F}{\partial V^2}\right)_T = V\left(\frac{\partial^2 E_{tot}}{\partial V^2}\right) + V\left(\frac{\partial^2 F_{vib}(a,T)}{\partial V^2}\right)_T. \tag{10}$$

The second derivatives in Eq. (10) are obtained via numerical differentiation and the results are compared with the available experimental data in Figs. 11 and 12. Both the values and the trend, a small decrease with

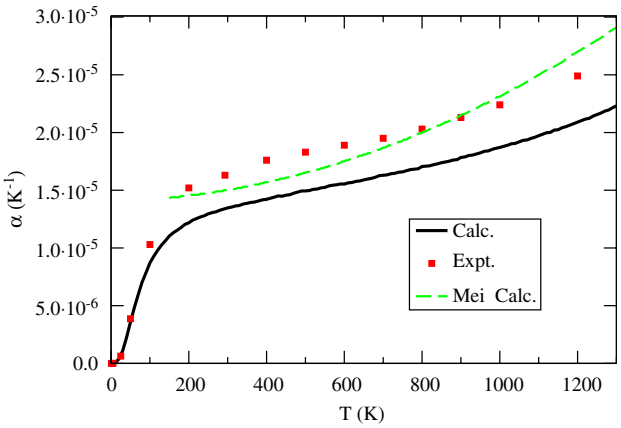

Fig. 8. Coefficient of linear thermal expansion $\alpha(T)$ as a function of temperature for Cu. The solid line represents the calculated values, the square points are the experimental values from Ref. [57], and the dashed line represents the results of the MD simulation of Mei et al. [33].

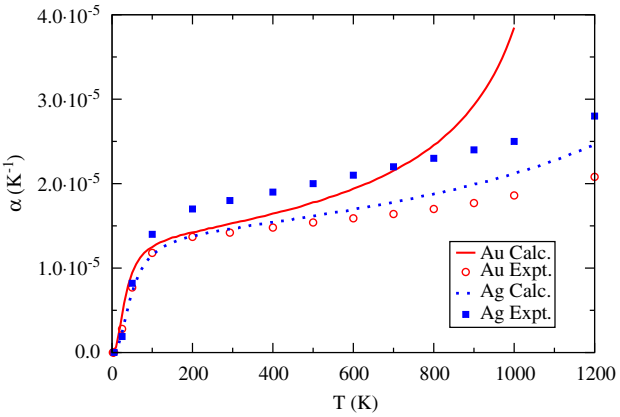

Fig. 9. Coefficient of linear thermal expansion $\alpha(T)$ as a function of temperature for Ag and Au. The lines represent the calculated values, and the symbols represent the experimental values from Ref. [57].

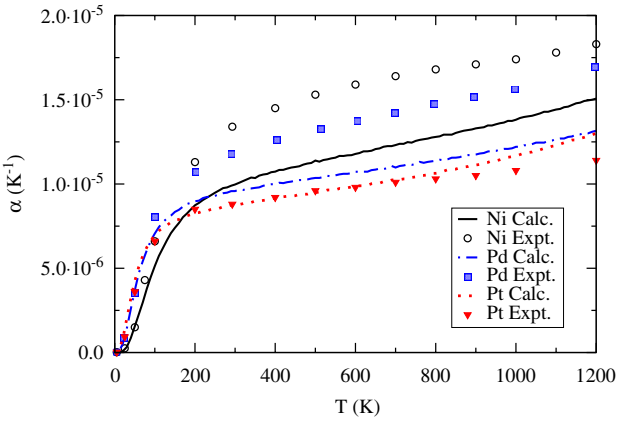

Fig. 10. Coefficient of linear thermal expansion $\alpha(T)$ as a function of temperature for Ni, Pd and Pt. The lines represent the calculated values, and the symbols represent the experimental values from Ref. [57].

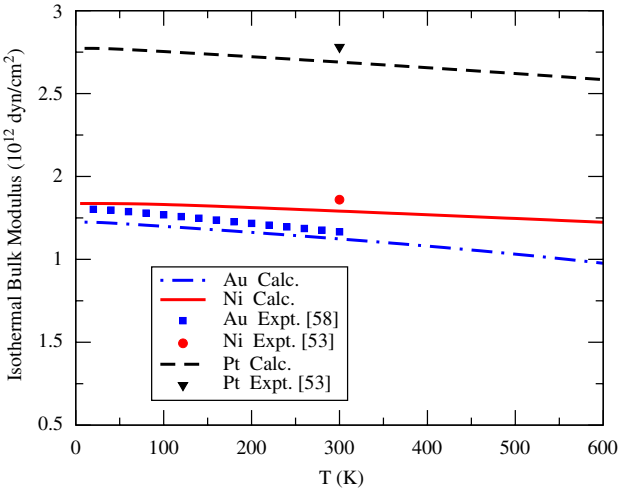

Fig. 11. Isothermal bulk modulus $B(T)$ as a function of temperature for Au, Ni and Pt. Experimental data are taken from Refs. [53] and [58].

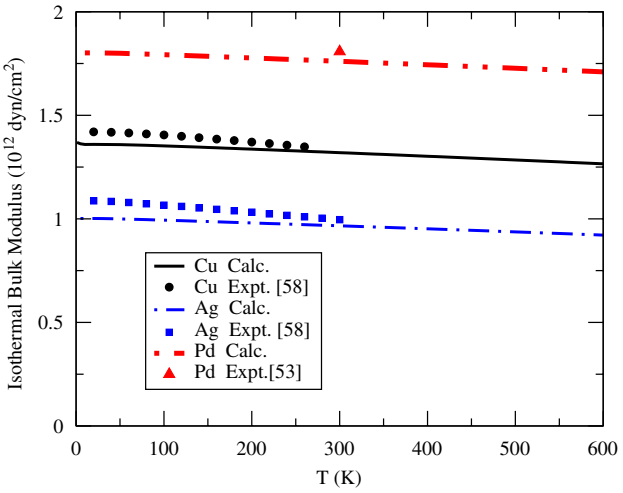

Fig. 12. Isothermal bulk modulus $B(T)$ as a function of temperature for Ag, Cu and Pd. Experimental data are taken from Refs. [53] and [58].

increasing temperature, are reproduced reasonably well in the calculation.

The specific heat at constant volume C_V can be obtained from the temperature derivative of the total energy. However, the contribution from the electrons excited across the Fermi level cannot be obtained from the EAM expression. Hence we write the specific heat at constant volume as

$$C_V(T) = C_V^{ph}(T) + C_V^{el}(T), \tag{11}$$

where the phonon part is obtained from the EAM model via

$$C_V^{ph}(T) = k_B \sum_{\mathbf{K}s} \left\{ \frac{\hbar\omega_s(\mathbf{K})}{2k_BT} \right\}^2 \frac{1}{\sinh^2[\hbar\omega_s(\mathbf{K})/2k_BT]}. \tag{12}$$

We estimate the electronic part $C_V^{el}(T)$ via the well-known expression:

$$C_V^{el}(T) = \frac{\pi^2}{3} k_B^2 N(E_F) T, \tag{13}$$

where $N(E_F)$ is the electronic DOSs at the Fermi level E_F. In the above expressions we consider the specific heats and $N(E_F)$ to be per atom. We use the well-known and well-documented Stuttgart TB-LMTO (tight binding linear muffin-tin orbitals) code [49] to compute the values of $N(E_F)$ for various lattice parameters. For the benefit of readers not familiar with the method, a brief description of the linear muffin-tin orbitals (LMTO) method and its tight-binding version (TB-LMTO) is provided as an Appendix. Our results agree well with those given by other methods [50]. With increasing temperature, the lattice parameter increases and electronic bands become narrower, resulting in a slight increase in $N(E_F)$. However, this increase is negligible and the variation of $C_V^{el}(T)$ with temperature remains essentially linear. We have actually calculated the $N(E_F)$ for 5–6 values of lattice parameters in the entire temperature range and used linear interpolation to find the values at all other lattice parameters. Note that for the transition metals, Ni, Pd and Pt, with substantial d-state DOS at the Fermi level, the agreement with the experimental results cannot be obtained without the electronic contribution.

Eq. (13), which is based on the independent fermionic quasiparticle picture [51,52], includes all the electron–ion, exchange and correlation effects as incorporated within the framework of density functional theory. What is neglected is the electron–phonon interaction [51,52], which is presumably small for most of the metals considered, as none of these exhibits superconductivity down to almost absolute zero of temperature. Linear response calculations of electron–phonon interaction based on the full-potential LMTO method by Savrasov and Savrasov [40] show that for Cu it is indeed negligible, while for Pd it may not be entirely negligible (electron–phonon coupling constant $\sim$0.3). Since the values of the electron–phonon coupling constant are known only for a few of these metals and are expected to be small ($<$0.15) for all metals except for Pd, we have not included this contribution. In any case, based on Savrasov's [40] results, we estimate that the electron–phonon interaction will cause the specific heat to be larger by about 10% or less for most of these metals, while for Pd the correction may be $\sim$30%. These estimates should be considered with appropriate caution. In principle, the electron–phonon part of the specific heat must be consistent with the phonon or the lattice part. Since we have calculated the lattice part using the EAM and the estimates of 10–30% are based on the LMTO method, it would be somewhat inappropriate for us to add these corrections arbitrarily to the calculated specific heat. The purpose of considering the electronic specific heat is simply to show that this contribution is important for all the transition metals (Ni, Pd and Pt) and small for the noble

metals (Cu, Ag and Au). The experimental values contain the effects of electron–phonon interaction in addition to the contributions from vacancies [47] and other defects. Note that in the high temperature limit the calculated quasiharmonic value of $C_V^{ph}(T)$ reaches the classical harmonic value $3k_B$ per atom, as it should.

We calculate the specific heat at constant pressure C_P by using the relation:

$$C_P(T) - C_V(T) = -T\left(\frac{\partial V}{\partial T}\right)_P^2 \left(\frac{\partial P}{\partial V}\right)_T, \tag{14}$$

or

$$C_P(T) = C_V^{ph}(T) + C_V^{el}(T) + \tfrac{9}{4}\alpha^2(T)B(T)a_e^3(T)T. \tag{15}$$

Figs. 13–18 show the temperature-dependence of heat capacity at constant volume C_V^{ph}, at constant pressure C_P and the electronic contribution C_V^{el}. The experimental results, which are for C_P, are also shown. For Ni, Pd and Pt, where the Fermi level lies within (at the outer edge) the d-band, DOSs $N(E_F)$ is large, resulting in a substantial contribution to C_V. In most cases the agreement with the experimental results is good, except for Ni which is ferromagnetic below the Curie temperature T_c of 627 K [53]. The discrepancy between the calculated and experimental results is largest at the Curie temperature and decreases steadily for temperatures both below and above T_c. For both low and high temperatures, away from T_c, the agreement is very good. The discrepancy is understandable, as the present formulation of EAM does not distinguish between the magnetic and nonmagnetic states. For Cu (Fig. 14), the effects of anharmonicity can be seen in the dotted line, which represents the variation of C_P with temperature obtained by Mei et al. [33] using (classical) molecular dynamics simulation. The simulations contain anharmonic effects to all order, but the results are valid only at high temperature. Note that despite poor agreement between the calculated and measured phonon spectra for Au, the calculated and measured values of C_P agree very well over a large temperature range, possibly due to anharmonic effects excluded from the present calculation, which are, however, manifested in all measured properties. Poor phonon frequencies and anharmonic effects compensate for each other, yielding excellent values for C_P. Although the calculated phonon spectra for both Au and Pt show poor agreement with measured values, measured C_P for Au shows much better agreement with the calculated values than for Pt. On the contrary, measured thermal expansion is much better reproduced for Pt than for Au by the calculation.

The knowledge of C_P and C_V enables us to determine the adiabatic bulk modulus by using the relation $B_S(T) = (C_P/C_V)B(T)$. Calculated values of B_S decrease

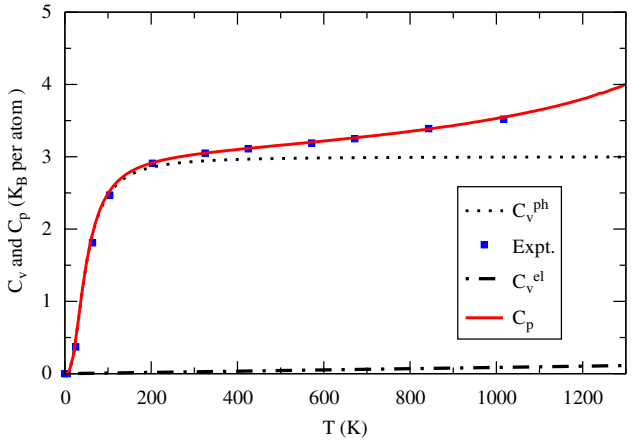

Fig. 13. Calculated temperature-dependence of heat capacity of Ag at constant volume C_V^{ph}, at constant pressure C_P and the electronic contribution C_V^{el}. The square points represent the experimental data for heat capacity at constant pressure from Ref. [59].

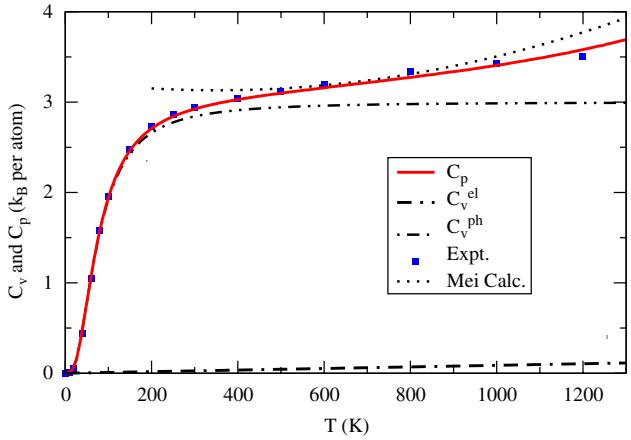

Fig. 14. Calculated temperature-dependence of heat capacity of Cu at constant volume C_V^{ph}, at constant pressure C_P and the electronic contribution C_V^{el}. The square points are the experimental data for heat capacity at constant pressure from Ref. [59]. The dotted line denotes the results from the molecular dynamics simulation of Ref. [33].

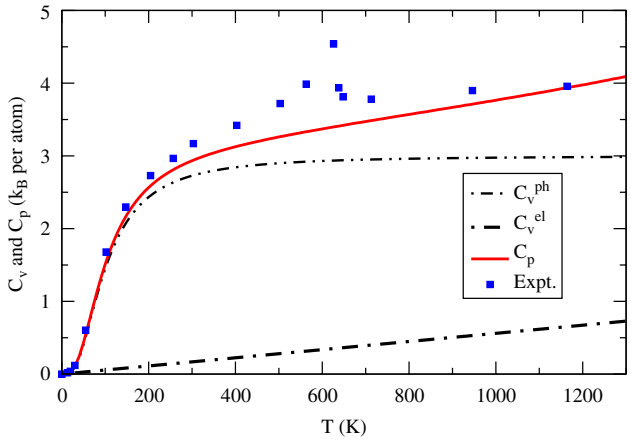

Fig. 15. Calculated temperature-dependence of heat capacity of Ni at constant volume C_V^{ph}, at constant pressure C_P and the electronic contribution C_V^{el}. The square points are the experimental data for heat capacity at constant pressure from Ref. [59].

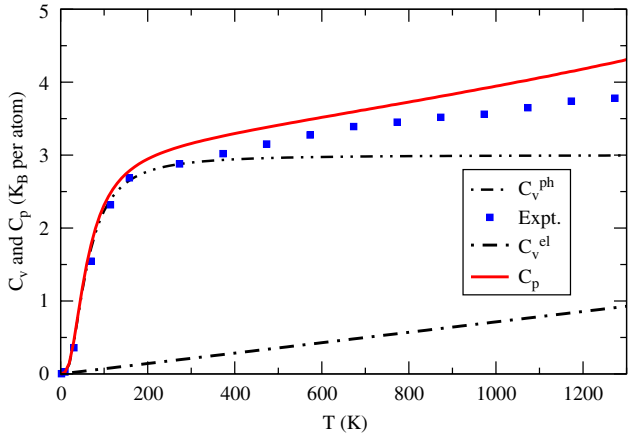

Fig. 16. Calculated temperature-dependence of heat capacity of Pd at constant volume C_V^{ph}, at constant pressure C_P and the electronic contribution C_V^{el}. The square points are the experimental data for heat capacity at constant pressure from Ref. [59].

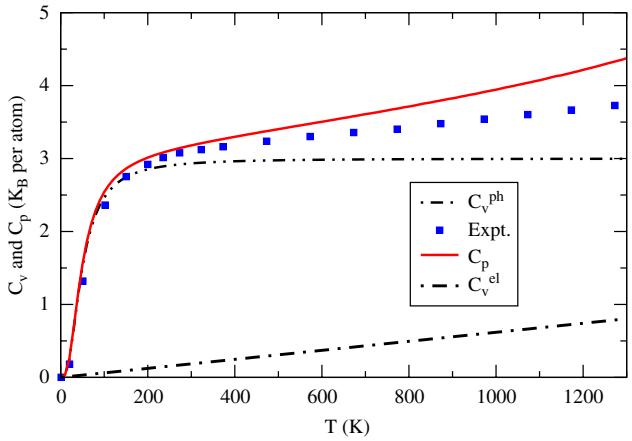

Fig. 17. Calculated temperature-dependence of heat capacity of Pt at constant volume C_V^{ph}, at constant pressure C_p and the electronic contribution C_V^{el}. The square points are the experimental data for heat capacity at constant pressure from Ref. [59].

linearly as a function of temperature. For Cu the values decrease from 1.36×10^{12} dynes/cm^2 at $T=0$ to 1.33×10^{12} dynes/cm^2 at 600 K, comparing favorably with the experimental value of 1.37×10^{12} dynes/cm^2 at room temperature and 1.42×10^{12} dynes/cm^2 at very low T [61]. For Ag the calculated values decrease from 1.002×10^{12} dynes/cm^2 at $T=0$ to 0.977×10^{12} dynes/cm^2 at 600 K, while the experimental values at low and room temperatures are 1.087×10^{12} and 1.043×10^{12} dynes/cm^2, respectively [60]. For Au the calculated values drop from 1.73×10^{12} dynes/cm^2 at $T=0$ to 1.66×10^{12} dynes/cm^2 at 600 K. The experimental values [60] at room and low temperatures are 1.75 and 1.80×10^{12} dynes/cm^2, respectively. The calculated values for Ni, Pd, and Pt show similar good agreement with the experimental values.

An important thermodynamic property is the Grüneisen parameter, which is essentially a measure of the volume-

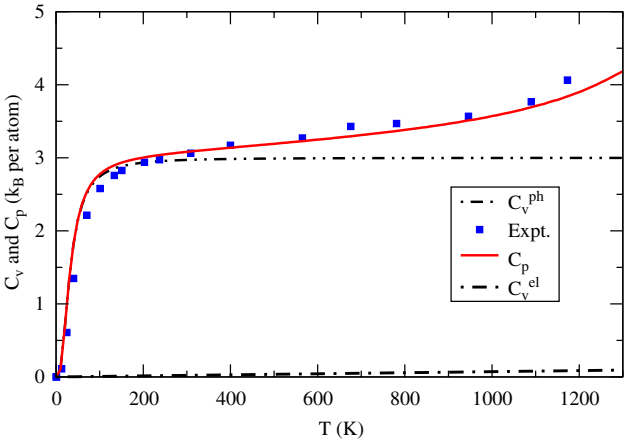

Fig. 18. Calculated temperature-dependence of heat capacity of Au at constant volume C_V^{ph}, at constant pressure C_P and the electronic contribution C_V^{el}. The square points are the experimental data for heat capacity at constant pressure from Ref. [59].

dependence of the phonon frequencies and can be related to thermal expansion of the solid. The mode-specific Grüneisen parameter corresponding to the $(\mathbf{K},s)$ phonon mode is given by

$$\gamma_s(\mathbf{K}) = -\frac{V}{\omega_s(\mathbf{K})}\frac{\partial\omega_s(\mathbf{K})}{\partial V}. \tag{16}$$

We compute the overall Grüneisen parameter $\gamma(T)$ by averaging over the individual Grüneisen parameters $\gamma_s(\mathbf{K})$ of all the modes with a weight of $C_V(\mathbf{K}s)$ from each mode$(\mathbf{K}s)$, i.e.,

$$\gamma(T) = \frac{\sum_{\mathbf{K}s}\gamma_s(\mathbf{K})C_V(\mathbf{K}s)}{\sum_{\mathbf{K}s}C_V(\mathbf{K}s)}. \tag{17}$$

Calculated $\gamma(T)$ increases monotonically with temperature for all the metals. For Cu the calculated value increases from 1.5 at 300 K to 1.85 at 1200 K, while the experimental values at 160 and 100 K are 1.9 and 2.2, respectively [47]. For Ag the calculated value increases from 1.5 at 300 K to 1.95 at 1200 K. The experimental value at room temperature is 2.3 [47]. For Au calculated and experimental [62] values at room temperature are 2.9 and 3.0, respectively. For Ni the calculated value increases from 1.5 at room temperature to 1.8 at 1200 K, comparing favorably with the experimental room temperature value 1.7 [62]. Calculated and experimental [62] room temperature values for Pd are 1.75 and 2.2, and for Pt they are 2.6 and 2.7, respectively.

Finally, we study the Debye temperature and its temperature-dependence. The temperature dependent Debye temperature Θ_D is obtained by numerically evaluating the integral

$$C_V(T) = 9k_B\left(\frac{T}{\Theta_D}\right)^3\int_0^{X_D}\frac{X^4\exp(X)}{[\exp(X)-1]^2}\,dX, \tag{18}$$

with $X_D=\Theta_D/T$, and adjusting the value of X_D so that the integral on the right-hand side of Eq. (18) matches the

already computed value of $C_V(T)$ on the left-hand side. The calculated values are slightly smaller than the corresponding experimental values [53,63–65] reflecting the difference between the calculated and the measured values of C_V. However, the maximum difference is of the order of 10%. For all metals there is an initial decrease in the Debye temperature as the temperature increases from zero, except for Au where there is an initial increase. This is shown in Fig. 19, where the Debye temperatures of three noble metals are compared with the experimental results. It is interesting that the present EAM model is able to capture this trend. All previous calculations, based on two-body potentials alone, had failed to produce the initial increase of the Debye temperature for Au.

It would be natural to compare the thermodynamic properties of the metals among themselves by dividing them into two isoelectronic groups: Ni, Pd, Pt (transition metals) and Cu, Ag, Au (noble metals). Most of the thermodynamic properties follow a definite trend within a given group. For example, the co-efficient of thermal expansion of the transition metal group is on average less than that of the noble metal group. Within a group the coefficient of thermal expansion increases monotonically from 3*d* to 5*d* metals. The Grüneisen parameter, being approximately proportional to thermal expansion, seems to follow the same trend. The Debye temperature of the transition metal group is higher on average than the noble metal group, with a monotonic decrease from 3*d* to 5*d* metals. The variation within a group as well as between the two groups can in principle be explained based on the mass of the elements and the bonding properties which are dependent on the electronic structure, including relativistic effects for Au and Pt. It appears that the present EAM model can reproduce the trend qualitatively. It is particularly interesting that the small initial increase in Debye temperature of Au with increasing temperature, which is an exception among all the metals studied, is reproduced by the model. Earlier studies based purely on two body-potentials have failed to reproduce this feature.

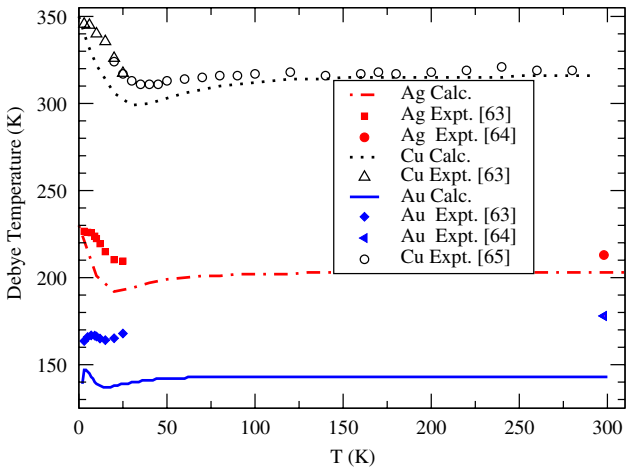

Fig. 19. Debye temperature Θ_D as a function of temperature T for Cu, Ag and Au.

5. Summary of results and conclusions

This work presents the first complete study of the phonon dispersion curves and all thermodynamic properties of the afore-mentioned metals, based on the EAM potential of Mei et al. [33] The calculated phonon dispersion curves for Cu and Ag agree well with the INS results. The discrepancy between the calculated and the measured phonon frequencies increases with increasing phonon wave vector for all of the above metals. However, the relative error, at the symmetry points X and L, is not more than 5.0% for Ag and 7.0% for Cu. Large differences between the calculated and the measured phonon frequencies are found for Ni, Pd, Pt and Au at high values of phonon frequencies, with the discrepancy for Au being the most drastic. However, the agreement or the lack thereof in the calculated phonon dispersion curves does not carry over to the thermodynamic properties in a proportionate way. For example, despite poor agreement for the phonon frequencies, the calculated and measured values of C_P agree very well for Au over a wide temperature range. Although the calculated phonon dispersion curves for both Au and Pt show poor agreement with measured values, measured C_P for Au shows much better agreement with the calculated values than for Pt. On the contrary, measured thermal expansion is much better reproduced for Pt than for Au by the calculation.

For the transition metals, Ni, Pd and Pt, with substantial *d*-state DOSs at the Fermi level, it is essential to include the electronic contribution to the specific heat, in order to achieve agreement with the measured values.

Both isothermal and adiabatic bulk moduli are very well represented over a wide temperature range for all the metals studied. In general, the co-efficient of thermal expansion, calculated in the quasiharmonic approximation, is underestimated for most of the metals beyond room temperature. Calculated values of C_P for Ag, Cu and Au agree very well with the measured values. For Ni the agreement is good both below and above the Curie temperature, with the discrepancy increasing as the Curie temperature is approached from both above and below. This is understandable as the present model of EAM is not designed to capture the physics of a ferromagnetic to paramagnetic transition. The Grüneisen parameter and Debye temperature are underestimated by about 10% for all the metals. However, the temperature variation of the Debye temperature, an initial decrease as the temperature is raised from zero for all the metals except Au, is reproduced well by the model. For Au the experimental values of the Debye temperature show an initial increase. This feature is also captured by the model.

In summary, the temperature-dependence of the thermodynamic properties of the six fcc metals studied is reproduced reasonably well by the EAM model of Mei

et al. [33]. The coefficient of thermal expansion is underestimated above the room temperature in the quasiharmonic approximation used in this work. Inclusion of the anharmonic effects may improve the results. Comparison of our quasiharmonic results for thermal expansion of Cu with the molecular dynamics results of Mei et al. [33] in Fig. 7 shows that for Cu the anharmonic effects are actually small. The same conclusion for Cu is reached via a comparison of C_P values (Fig. 14). There is room for much improvement in the phonon dispersion curves for Ni, Pd, Pt and Au. It is somewhat surprising that this model, where the parameters for all the metals are determined in the same way, produces results that are so drastically disparate among the different metals in terms of agreement with the experimental data.

Acknowledgment

Financial support for this work was provided by Natural Sciences and Engineering Research Council of Canada.

Appendix A

A.1. LMTO and TB-LMTO

LMTO method has been described in various articles by Andersen and coworkers [49] and in great details in a monograph by Skriver [66]. In the LMTO method [49,66] space is divided into muffin-tin spheres centered at various atomic sites and the interstitial regions. For open structures, e.g. diamond, in addition to atomic spheres, empty spheres are placed at interstitial sites to render the space occupied by spheres close-packed. The potential inside the spheres is assumed to be spherically symmetric and is computed according to the prescription of the density functional theory. Outside the spheres the potential is assumed to be constant. The energy-independent basis set in the conventional or unscreened LMTO method consists of functions $\chi^0_{\vec{R}L}(\vec{r}-\vec{R})$ centered about the sites $\vec{R}$ in the solid, where $L(\equiv l,m)$ is the collective angular momentum index:

$$\chi^0_{\vec{R}L}(\vec{r}-\vec{R}) = K^0_{\vec{R}L}(\vec{r}-\vec{R}) + \Phi_{\vec{R}L}(\vec{r}-\vec{R}) + \sum_{\vec{R}',L'} \dot{\Phi}^0_{\vec{R}'L'}(\vec{r}-\vec{R}')h^0_{\vec{R}'L'\vec{R}L}. \quad (19)$$

Here $K^0_{\vec{R}L}$ is the envelope function which is supposed to vanish inside all the spheres, while in the interstitial region it is given by the solution of the one-electron Schrödinger equation with the electron energy equal to the muffin-tin zero of the potential. This choice of the electron energy reduces the Schrödinger equation to the Laplace equation in the interstitial region. $K^0_{\vec{R}L}$ is thus taken to be proportional to $|\vec{r}-\vec{R}|^{-l-1}Y_L(\theta,\phi)$, the solution of the Laplace equation that is irregular at $\vec{R}$ but regular at infinity. It is the field of a 2^l pole situated at the site $\vec{r}$. The functions $\Phi_{\vec{R}L}$ and $\dot{\Phi}^0_{\vec{R}L}$ are supposed to vanish outside the sphere at $\vec{R}$. $\Phi_{\vec{R}l}$, the angular part of $\Phi_{\vec{R}L}$, is the normalized solution of the radial part of the wave equation for orbital angular momentum l inside the sphere at $\vec{R}$ for a reference energy E_{vRl}, and $\dot{\Phi}^0_{\vec{R}l}$ is a linear combination of $\Phi_{\vec{R}l}$ and its energy derivative at the energy E_{vRl}. LMTOs defined by Eq. (19) provide an accuracy to linear order in the deviation $(E-E_{vRl})$ in the wave functions and to order $(E-E_{vRl})^2$ in the energy eigenvalues.The most commonly used choice of the reference energies is the centers of gravities of the occupied parts of the respective l-bands. This choice is found to reproduce the one-electron DOSs accurately over the entire occupied band, i.e. from the bottom of the band to the Fermi energy. The quantities $h^0_{\vec{R}'L'\vec{R}L}$ in Eq. (19) and the functions $\dot{\Phi}^0_{\vec{R}L}$ are chosen to ensure the continuity and the differentiability of the basis functions $\chi^0_{\vec{R}L}$ at the surfaces of all the spheres.

The eigenvalue problem for the solid is treated by writing the eigenfunctions as linear combinations of the LMTOs given by Eq. (19), which form the basis set for the conventional variational calculation. The solution to the eigenvalue problem is often simplified by using the atomic sphere approximation (ASA), which replaces the muffin-tin spheres with space-filling (and hence slightly overlapping) Wigner–Seitz (WS) spheres. The Hamiltonian and the overlap matrices in LMTO-ASA thus receive no contribution from the interstitial regions, i.e. there are no matrix elements involving the envelope functions $K^0_{\vec{R}L}$. The envelope functions, however, affect the $\Phi_{\vec{R}L}$, $\dot{\Phi}^0_{\vec{R}l}$ functions via their continuous and differentiable augmentation inside the spheres by these functions. In a nearly orthogonal LMTO representation, under ASA, the Hamiltonian matrix elements can be written as

$$H_{RL,R'L'} = E_{vRl}\delta_{RR'}\delta_{LL'} + h^0_{RL,R'L'} \quad (20)$$

$$= C_{RL}\delta_{RR'}\delta_{LL'} + \Delta^{1/2}_{RL}[S^0(1-\gamma S^0)^{-1}]_{RL,R'L'}\Delta^{1/2}_{R'L'}. \quad (21)$$

The properties of the atoms enter the Hamiltonian matrix H via the matrices $X(X=C,\Delta,\gamma)$, which are diagonal in the indices $\vec{R}$ and L and are independent of m, i.e.

$$(X)_{RL,R'L'} = X_{RL}\delta_{RR'}\delta_{LL'} = X_{Rl}\delta_{RR'}\delta_{LL'}.$$

Also $X_{Rl} = X^Q_l$, where Q is the type of the atom occupying the site $\vec{R}$. The matrix elements X_{RL} are called the potential parameters and can be derived from the knowledge of the functions $\Phi_{\vec{R}l}$ and their energy derivative at the reference energy E_{vRl}. S^0 is the canonical structure constant matrix, which depends on the relative positions of the sites, but is independent of the type of atoms that occupy the sites. This so-called 'bare' structure constant matrix arises from the expansion of the envelope function $K^0_{\vec{R}L}$ centered at $\vec{R}$ about all the neighboring sites $\vec{R}'$. Because of the

long-range power law decay of the envelope function $K^0_{\vec{R}L}$ matrices S^0 and $\tilde{S} = [S^0(1-\gamma S^0)^{-1}]$ are long-ranged.

In the TB-LMTO method one uses envelope functions which are irregular not only at the central site but also at the neighboring sites. In this way the field due to the multipole at the central site is screened by similar fields from the surrounding sites. A diagonal "screening matrix", $\alpha_{RL,R'L'} = \alpha_{RL}\delta_{RR'}\delta_{LL'}$, is introduced in the theory. The resulting screened or short-ranged envelope functions give rise to short-ranged basis functions and short-ranged Hamiltonian matrix elements with the same form as in Eq. (2):

$$H^{\alpha}_{RL,R'L'} = E_{\nu Rl}\delta_{RR'}\delta_{LL'} + h^{\alpha}_{RL,R'L'} \tag{22}$$

$$= C^{\alpha}_{RL}\delta_{RR'}\delta_{LL'} + (\Delta^{\alpha}_{RL})^{1/2} \times [S^0(1-\alpha S^0)^{-1}]_{RL,R'L'}(\Delta^{\alpha}_{R'L'})^{1/2}. \tag{23}$$

A single site-independent, but l-dependent screening constant matrix, with only three nonzero elements corresponding to $l = 0, 1$ and 2 has been found to reproduce satisfactory results for all close-packed structures [67]. The screened structure constants $S^{\alpha} = S^0(1-\alpha S^0)^{-1}$ can thus be calculated, once for all, for a given structure, irrespective of the types of the atoms occupying the sites. For all close-packed structures the elements of the screened structure constant matrix are found to be practically zero beyond the second shell of neighbors. In the Stuttgart TB-LMTO code for crystalline solids the structure constants and the Hamiltonian are first calculated in the TB-LMTO basis. The eigenvalues and eigenvectors of the LMTO-ASA Hamiltonian in the orthogonal representation are obtained from those of the TB-LMTO Hamiltonian using analytic relations. The relationships between the LMTO and TB-LMTO structure constants, potential parameters and the Hamiltonians are described in the articles by Andersen [49]. Bose and co-workers have carried out several applications of the TB-LMTO Hamiltonians to liquid metals and amorphous systems [68–71].

References

[1] P.C. Gehlen, J.R. Beeler, R.I. Jaffee (Eds.), Interatomic Potentials and the Simulation of Lattice Defects, Plenum, New York, 1972.

[2] A.E. Carlsson, C.D. Gelatt Jr., H. Ehrenreich, Philos. Mag. A 41 (1980) 241;
See also A.E. Carlsson, in: H. Ehrenreich, D. Turnbull (Eds.), Beyond Pair Potentials in Solid State Physics, vol. 43, Academic Press, New York, 1990, p. 1.

[3] E.R. Cowley, R.C. Shukla, Phys. Rev. B 9 (1974) 1261.

[4] M.W. Finnis, J.E. Sinclair, Philos. Mag. A 50 (1984) 45.

[5] B. Legrand, Philos. Mag. B 49 (1984) 171.

[6] V. Rosato, M. Guilope, B. Legrand, Philos. Mag. A 59 (1989) 321 and references therein.

[7] D.G. Pettifor, in: H. Ehrenreich, D. Turnbull (Eds.), Solid State Physics, vol. 40, Academic Press Inc., New York, 1987, p. 43.

[8] F. Ducastelle, F. Cyrot-Lackmann, J. Phys. Chem. Solids 32 (1971) 285.

[9] R.P. Gupta, Phys. Rev. B 23 (1981) 6265.

[10] D. Tománek, S. Mukherjee, K.H. Bennemann, Phys. Rev. B 28 (1983) 665.

[11] D.G. Pettifor, Bonding and Structure of Molecules and Solids, Oxford Science Publications, 2002 (Chapter 7);
See also A.P. Sutton, Electronic Structure of Materials, Clarendon Press, Oxford, 2004 (Chapter 9).

[12] M.S. Daw, M.I. Baskes, Phys. Rev. B 29 (1984) 6443.

[13] M. Manninen, Phys. Rev. B 34 (1986) 8486.

[14] K.W. Jacobsen, J.K. Nørskove, M.J. Puska, Phys. Rev. B 35 (1987) 7423.

[15] S.M. Foiles, Phys. Rev. B 32 (1985) 3409.

[16] J. Mei, J.W. Davenport, Phys. Rev. B 42 (1991) 9682.

[17] J. Mei, J.W. Davenport, Phys. Rev. B 46 (1992) 21.

[18] S.M. Foiles, M.I. Baskes, M.S. Daw, Phys. Rev. B 33 (1986) 7983.

[19] R.A. Johnson, Phys. Rev. B 37 (1988) 3924;
R.A. Johnson, Phys. Rev. 39 (1989) 12554;
R.A. Johnson, Phys. Rev. 41 (1990) 9717.

[20] M.S. Daw, R.D. Hatcher, Solid State Commun. 56 (1985) 697.

[21] J.S. Nelson, E.C. Sowa, M.S. Daw, Phys. Rev. Lett. 61 (1988) 1977.

[22] J.S. Nelson, M.S. Daw, E.C. Sowa, Phys. Rev. B 40 (1989) 1465.

[23] M.S. Daw, S.M. Foiles, J. Vac. Sci. Technol. A 4 (1986) 1412.

[24] S.M. Foiles, Surf. Sci. 191 (1987) L779.

[25] T.E. Felter, S.M. Foiles, M.S. Daw, R.H. Stulen, Surf. Sci. 171 (1986) L379.

[26] M.S. Daw, S.M. Foiles, Phys. Rev. B 35 (1987) 2128.

[27] M.S. Daw, S.M. Foiles, Phys. Rev. Lett. 59 (1987) 2756.

[28] S.M. Foiles, Surf. Sci. 191 (1987) 329.

[29] M.I. Baskes, Phys. Rev. B 46 (1992) 2727.

[30] M.S. Daw, S.M. Foiles, M.I. Baskes, The embedded-atom method: a review of theory and applications, Materials Science Reports, Rev. J. 9 (1993) 251–310.

[31] S.M. Foiles, J.B. Adams, Phys. Rev. B 40 (1989) 5909.

[32] D.J. Oh, R.A. Johnson, J. Mater. Res. 3 (1988) 471.

[33] J. Mei, J.W. Davenport, G.W. Fernando, Phys. Rev. B 43 (1991) 4653.

[34] C. Kuiying, L. Hongbo, L. Xiaoping, H. Qiyong, H. Zhuangqi, J. Phys. Condens. Matter 7 (1995) 2379.

[35] J.H. Rose, J.R. Smith, F. Guinea, J. Ferrante, Phys. Rev. B 29 (1984) 2963.

[36] Y.P. Varshni, F.J. Bloore, Phys. Rev. 129 (1963) 115.

[37] E.C. Svensson, B.N. Brockhouse, J.M. Rowe, Phys. Rev. 155 (1967) 619.

[38] See, e.g., M. Born, K. Huang, Dynamical Theory of Crystal Lattices, Oxford University Press, Oxford, 1962, p. 142.

[39] G. Nilsson, S. Ronaldson, Phys. Rev. B 7 (1973) 2393.

[40] See, for example, S.Y. Savrasov, D.Y. Savrasov, The full potential linear muffin-tin (FP-LMTO) results for Cu and Pd, Phys. Rev. B 54 (1996) 16487.

[41] See Y. Mishin, M.J. Mehl, D.A. Papaconstantopoulos, A.F. Voter, J.D. Kress, Phys. Rev. B 63 (2001) 224106.

[42] See, for example, S. Narasimhan, S. de Gironcoli, The pseudopotential-based results for Cu, Phys. Rev. B 65 (2002) 064302. The results are somewhat inferior to those based on the FP-LMTO method of Ref. [S.Y. Savrasov, D.Y. Savrasov, The full potential linear muffin-tin (FP-LMTO) results for Cu and Pd, Phys. Rev. B 54 (1996) 16487] or the *ab initio* tight-binding results of Ref. [Y. Mishin, M.J. Mehl, D.A. Papaconstantopoulos, A.F. Voter, J.D. Kress, Phys. Rev. B 63 (2001) 224106], and also seem to depend on the scheme, LDA (local density approximation) vs. GGA (generalized gradient approximation), used to treat the exchange-correlation potential.

[43] D.H. Dutton, B.N. Brockhouse, A.P. Miiller, Can. J. Phys. 50 (1972) 2915.

[44] Y. Mishin, D. Farkas, M.J. Mehl, D.A. Papaconstantopoulos, Phys. Rev. B 59 (1999) 3393.

[45] S. Chantasiriwan, F. Milstein, Phys. Rev. B 58 (1998) 5996.

[46] W.A. Kamitakahara, B.N. Brockhouse, Phys. Lett. 29A (1980) 639.

[47] R.A. MacDonald, W.M. MacDonald, Phys. Rev. B 24 (1980) 1715.

[48] R.C. Shukla, R.A. MacDonald, High Temp.-High Press. 12 (1980) 291.
[49] O.K. Andersen, Phys. Rev. B 8 (1975) 3060;
O.K. Andersen, O. Jepsen, D. Glötzel, in: F. Bassani, F. Fumi, M.P. Tosi (Eds.), Highlights of Condensed Matter Theory, North-Holland, Amsterdam, 1985, pp. 59–176;
O.K. Andersen, O. Jepsen, M. Sob (Eds.), in: M. Yossouff (Ed.), Electronic Structure and its Applications, Lecture Notes in Physics, vol. 283, Springer, Berlin, 1987, pp. 1–57;
See also ⟨http://www.fkf.mpg.de/andersen/⟩.
[50] See for example V.L. Moruzzi, J.F. Janak, A.R. Williams, Calculated Electronic Properties of Metals, Pergamon, New York 1978; D.A. Papaconstantopoulos, Handbook of the Band Structure of Elemental Solids, Plenum, New York, 1986.
[51] G. Grimvall, The Electron–Phonon Interaction in Metals, North-Holland, Amsterdam, 1981 (Chapter 6).
[52] R.E. Prange, L.P. Kadanoff, Phys. Rev. 134 (1964) A566.
[53] C. Kittel, Introduction to Solid State Physics, Wiley, New York, 1996.
[54] J.W. Lynn, H.G. Smith, R.M. Nicklow, Phys. Rev. B 8 (1973) 3493.
[55] R.J. Birgeneau, J. Cordes, G. Dolling, A.D.B. Woods, Phys. Rev. 136 (1964) A1359.
[56] A.P. Miiller, B.N. Brockhouse, Can. J. Phys. 49 (1971) 704.
[57] Y.S. Touloukian, R.K. Kirby, R.E. Taylor, P.D. Desai, Thermophysical Properties of Matter, The TPRC Data Series, Thermal Expansion, Metallic Elements and Alloys, Plenum Data Company, New York, 1977.
[58] D.C. Wallace, Thermodynamics of Crystals, Wiley, Toronto, 1972.
[59] Y.S. Touloukian, E.H. Buyco, Thermophysical Properties of Matter, The TPRC Data Series, Specific Heat, Metallic Elements and Alloys, vol. 4, Plenum Data Company, New York, 1970.
[60] J.R. Neighbors, G.A. Alers, Phys. Rev. 111 (1958) 707.
[61] W.C. Overton Jr., J. Gaffney, Phys. Rev. 98 (1955) 969.
[62] C.V. Pandya, P.R. Vyas, T.C. Pandya, V.B. Gohel, Bull. Mater. Sci. 25 (2002) 63.
[63] D.L. Martin, Phys. Rev. 141 (1966) 576.
[64] W.D. Compton, K.A. Gschneidner, M.T. Hutchings, H. Rabin, M.P. Tosi, Solid States Physics, Advances in Research and Applications, vol. 16, Academic Press, New York, 1964.
[65] D.L. Martin, Can. J. Phys. 38 (1960) 2049.
[66] H.L. Skriver, The LMTO Method, Springer Series in Solid-State Sciences, vol. 41, Springer, Berlin, 1984.
[67] O.K. Andersen, O. Jepsen, Phys. Rev. Lett. 53 (1984) 2571.
[68] S.K. Bose, K. Weiner, O.K. Andersen, Phys. Rev. B 37 (1988) 6262.
[69] S.K. Bose, S.S. Jaswal, O.K. Andersen, J. Hafner, Phys. Rev. B 37 (1988) 9955.
[70] S.K. Bose, O. Jepsen, O.K. Andersen, Phys. Rev. B 48 (1993) 4265.
[71] S.K. Bose, Metall. Mater. Trans. A 29A (1998) 1853.